

1 **No Internal Connections Detected Between Leading Decadal to Multidecadal**
2 **Climate Modes in North Atlantic and North Pacific Basins**

3

4 **T. Fenske¹ and A. Clement¹**

5 ¹Rosenstiel School of Marine and Atmospheric Science, University of Miami, Miami, Florida

6

7 Corresponding author: Tyler Fenske (tyler.fenske@rsmas.miami.edu)

8

9 **Key Points:**

- 10 • Novel methods are applied to decadal to multidecadal climate modes to analyze possible
11 relationships between modes in different basins.
- 12 • An analysis of relationships between leading North Atlantic and North Pacific climate modes
13 does not reveal any internal connections, challenging previous results.
- 14 • External forcing such as global warming is shown to be a possible confounding factor in
15 climate relationships.

17

18

19

20

21

22

23

24

25

26

27

28

29

30 Abstract

31 Previous studies have attempted to unravel possible connections between leading decadal
32 to multidecadal climate modes in the North Atlantic and North Pacific ocean basins, the Atlantic
33 Multidecadal Variability in the North Atlantic, and the Pacific Decadal Oscillation and Victoria
34 Mode in the North Pacific. We use newly available climate model data and apply improvements
35 to existing methods to reexamine relationships among the different modes. Our main tool is the
36 Multi-Model Large Ensemble Archive, which includes 270 ensemble members and allows for
37 isolation of the forced and internal components of climate variability. Our results suggest that
38 any internal connections between these modes are indistinguishable from random noise. Further,
39 external forcing is shown to affect each region in similar ways, suggesting that climate change
40 could be an indirect link between the two basins, and can confound the interpretation of he
41 relationship between the basins.

42 Plain Language Summary

43 We examine possible connections between climate patterns in the North Atlantic and
44 North Pacific oceans. New climate model data and improved statistical methods allow us to build
45 on previous research of these links. In contrast to previous studies, no natural connections are
46 detected. However, global warming is shown to affect each region in similar ways, suggesting
47 that climate change could be an indirect link between the two basins.

48

49 Introduction

50 Climate modes are considered to be the leading source of internal climate variability,
51 affecting weather and climate patterns across the globe. These long-distance effects are
52 sometimes referred to as teleconnections and are driven by atmospheric bridges (Alexander et al.
53 2002, Liu and Alexander 2007). Sea-surface temperature (SST) variability associated with a
54 particular climate mode is coupled to the atmosphere, allowing the mode to change the overlying
55 atmospheric circulation. This signal is then transported through the atmosphere to other regions,
56 where the variability influences the ocean in a distant location, potentially imprinting on or even
57 exciting a different climate mode there (e.g. Liu and Alexander 2007, Dommegård and Latif
58 2008). The magnitude of control a climate mode has on another region can also vary in time,
59 adding another dimension to potential interactions and making them more difficult to identify
60 (Raible et al. 2014). The possibility of climate mode interactions must be considered to fully
61 understand the sources of internal climate variability.

62

63 Here, we focus on potential interactions between decadal to multidecadal climate modes
64 in the North Atlantic (NA) and North Pacific (NP) ocean basins. In the NA, low-frequency
65 variability is captured via the Atlantic Multidecadal Oscillation (AMO) or Atlantic Multidecadal
66 Variability (AMV) (Enfield et al. 2001). In the NP, two modes are commonly used to capture the
67 low-frequency variability. The Pacific Decadal Oscillation (Mantua et al. 1997) and the Victoria
68 Mode (VM) (Bond et al. 2003) or North Pacific Gyre Oscillation (NPGO) (Di Lorenzo et al.
69 2008) are the two leading modes of decadal and multidecadal variability respectively. Many
70 other methods of capturing variability in these basins have since been developed (Eden and Jung
71 2001, Salinger et al. 2001, Martin et al. 2019, Nigam et al. 2020, etc.), although convention has
72 maintained scientific usage of the AMV and PDO as the dominant low-frequency modes.

73 Despite their extensive usage, these modes, especially the AMV, may not adequately isolate and
74 capture a single source of internal variability (Marini and Frankignoul 2014; Wills et al. 2018;
75 O'Reilly et al. 2019, etc.). Representing multidecadal variability with relatively short observed
76 periods (order of 100 years) is also challenging, especially when low-pass filtering is applied
77 (Cane et al. 2017). Assuming oscillatory variability, only one or two full cycles may be observed
78 (Mann et al. 2021). This reduces the effective degrees of freedom and subsequently requires care
79 to be taken during statistical analysis, especially regarding significance testing.
80

81 Several previous studies have worked on the NA-NP relationship, all of which suggest
82 that the two basins have some statistical relationship with each other. Both d'Orgeville and
83 Peltier (2007) and Zhang and Delworth (2007) relate the first two Empirical Orthogonal
84 Functions or Principal Components (EOFs or PCs, hereafter referred to as EOFs) of NP SSTs to
85 a metric for the AMV (d'Orgeville and Peltier use the first EOF of NA SSTs, while Zhang and
86 Delworth use NA area mean SSTs), although they utilize those EOFs in different ways.
87 d'Orgeville and Peltier combine them and then isolate the 20 year (analogous to the PDO) and 60
88 year (analogous to the VM) period wavelets and conclude that there is a singular source driving
89 variability in each region, while Zhang and Delworth use the two EOFs and conclude that the
90 Atlantic Meridional Overturning Current (AMOC) drives the AMV, which in turn drives the
91 PDO/VM through atmospheric teleconnections. Wu et al. (2011) use the first two EOFs of each
92 basin and finds a statistically significant link. Marini and Frankignoul (2014) use several
93 methods attempting to deconstruct the origin of the AMV, such as dynamical filtering and
94 removing trends in various manners. Their analysis includes a comparison of the AMV and
95 PDO, where they come to a similar conclusion as previous studies. Nigam et al. (2020) uses
96 global rotated empirical orthogonal functions (EOFs) to represent all major global modes, and
97 their modes most similar to the AMV and PDO also support a relationship existing. An et al.
98 (2021) use ensemble pacemaker experiments to suggest that multidecadal Pacific variability is
99 generated by AMO forcing and local air-sea interactions. These studies use the student's t-test for
100 significance thresholds, with Wu et al. (2011) also using customized bootstrap methods. All of
101 these studies are in agreement that a modest but statistically significant correlation exists with the
102 AMV leading the PDO by 12-14 years.
103

104 Here we will build upon those previous examples using a novel dataset, the Multi-Model
105 Large Ensemble Archive (MMLEA), and improve on existing methods, such as significance
106 testing and mode definitions. Using these tools, we reanalyze the potential relationships between
107 low-frequency climate variability in the NA and NP ocean basins. Our results challenge previous
108 findings, suggesting that a relationship is not statistically significant. We also focus on the role
109 that external forcing plays in the inter-basin relationship and find that it may be a confounding
110 factor.
111

112 Data

113 For SST observational data, we use the UK Met Office's Hadley Centre Sea Ice and SST
114 data set (HADISST) (Rayner et al. 2003). Data is linearly detrended at each grid point, and we
115 use 151 years of monthly data from 1870-2020. We repeat our analysis with other common SST
116 datasets and find no qualitative differences.
117

Our primary tool is the new Multi-Model Large Ensemble Archive (MMLEA) (Deser et al. 2020). Necessary output is currently available for six ensembles included in the MMLEA (each hereafter as CANESM2, CESM, CSIRO-MK36, GFDL-CM3, GFDL-ESM2M, and MPI). Each ensemble contains at least 20 members for a total of 269 members (50, 39, 30, 20, 30, and 100 respectively). All MMLEA members are from the CMIP5 era and use historical forcing. Data from each member is cut off at the year 2020 to match the observed period. We also use each member's corresponding pre-industrial control run (PI), which are separate from the MMLEA. One advantage of large ensembles is their capability to extract the forced signal from each member by subtracting the ensemble mean (Kay et al. 2015). More details on the MMLEA are provided in Table S1 (adapted from Deser et al. 2020).

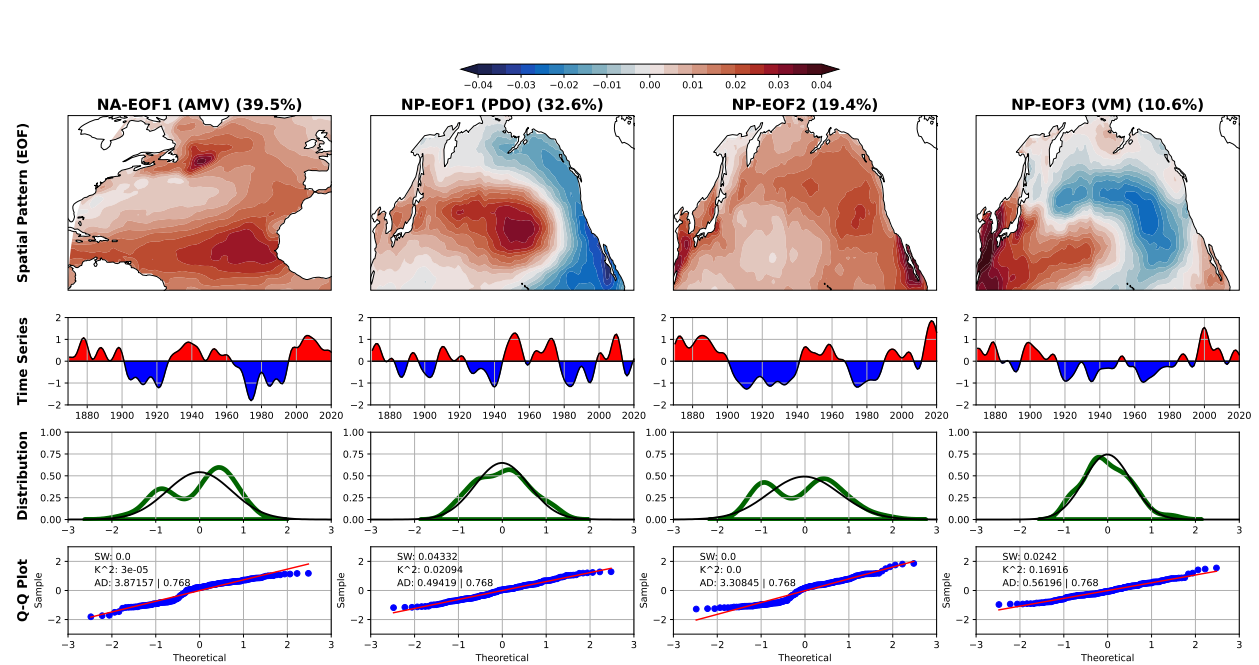
Mode Definitions

Our mode definitions for each basin loosely follow the conventions for the AMV, PDO, and VM (Enfield et al. 2001, Mantua et al. 1997, and Bond et al. 2003 respectively). Instead of applying unique methods (EOF analysis for the NP, regional area mean for the NA) to each basin, we apply EOF analysis to each basin in an attempt to better capture individual modes of variability. We compute the first three EOFs over the NP region of 20°N-65°N, 120°E-100°W and the first EOF over the NA region of 0°N-65°N, 120°W-0°. We also compute further EOFs for the NA, however these do not have as clear of a physical interpretation and do not affect our results in any meaningful way. They are not included except in Supplemental Figure 1, which shows a matrix of relationships between the first three EOFs of each basin, with no significant relationships involving any NA EOFs except the first. Figure 1 shows the spatial patterns of these EOF modes in the first row, while the second row shows the corresponding time series. NA-EOF1 represents the AMV, characterized by a tripole spatial pattern and a predominantly multi-decadal time series. NP-EOF1 represents the PDO, characterized by a dipole spatial pattern with warming (cooling) in the central NP and cooling (warming) along the eastern boundary, along with a mostly decadal time series. NP-EOF3 represents the VM, also characterized by a dipole pattern offset to the west from the PDO's, as well as a mostly decadal time series.

A major challenge in understanding climate mode drivers is separating internal variability from externally forced variability. This is typically achieved by removing the estimated forced trend. MMLEA data is detrended by removing the ensemble mean, following Deser et al. (2020). We define full variability (hereafter full) as the unmodified output of each member of the MMLEA, and we define internal variability as the full minus the ensemble mean. Observations are detrended linearly at each grid point, following convention. Figure 2 shows the effects of linear detrending on the EOF analysis in the NP. When no detrending occurs, the first EOF captures the externally forced global warming signal based on its uniform warming pattern, while the second EOF is clearly the PDO. Linear detrending causes the PDO to become the first EOF, while the second EOF still resembles the externally forced signal. Comparing the time series of these two apparent global warming signals reveals that they are remarkably similar. The second EOF of linearly detrended NP SSTs resembles the non-linear features of the global warming signal. Similar results exist for the NA (not shown). Other more complex detrending methods exist and offer different interpretations about what is forced versus what is internal, especially in the Atlantic (e.g. Frankignoul et al. 2017, Qin et al 2020). However, these differences in forced signals are not substantial enough to affect our results qualitatively.

164 Note that the composite mean and the ensemble mean are distinct and computed
 165 differently, namely in the order of operations because EOF analysis is a non-linear computation.
 166 Here, the composite mean is defined as EOF analysis being done first, followed by averaging of
 167 the EOFs. In contrast, the ensemble mean is where averaging is done first, and then EOF analysis
 168 is performed on the averaged SSTs. Physically, the ensemble mean represents the externally
 169 forced signal in each model, while the composite mean represents the average internal modes
 170 across all members.

171
 172 All time series are normalized and smoothed with a 10-year low-pass Lanczos filter to
 173 focus on decadal to multi-decadal variability, following classical methods.



176
 177 Figure 1. EOF modes and normality analysis of observed HadISST linearly-detrended North Atlantic and North Pacific SSTs.
 178 From left to right: NA-EOF1, NP-EOF1, NP-EOF2, and NP-EOF3. The percentage at the top of each column represents the
 179 variance explained by each EOF. NA-EOF1 is analogous to the AMV, NP-EOF1 to the PDO, and NP-EOF3 to the VM.
 180 NP-EOF2 is analogous to the non-linear global warming signal (more detail in text). Rows from top to bottom: 1) Spatial patterns of
 181 each EOF mode. Red (blue) corresponds to warming (cooling) when time series is positive (negative). 2) Filtered time series of
 182 each EOF mode. 3) Probability distribution of each time series are shown with shaded green curves; corresponding standard
 183 normal distributions are shown with black curves. 4) Quantile-quantile plots with data shown in blue points. A standard normal
 184 distribution is shown in red for comparison. Three quantitative assessments of normality are also applied: 1) The Shapiro-Wilk
 185 Test (SW). The corresponding p-value is listed, with p-values greater than 0.05 (95% confidence) implying a normal distribution.
 186 2) D'Agostino's K-Squared Test (K^2). The corresponding p-value is listed, with p-values greater than 0.05 (95% confidence)
 187 implying a normal distribution. 3) The Anderson-Darling Test (AD). The first value is the resulting measure of normality, and the
 188 second value is the 95% critical value for the AD test. If the first value is smaller than the critical value, the distribution can be
 189 assumed to be normal. All tests should be considered equally in determining whether or not to assume a normal distribution.

190 Normality of Modes

191 To determine whether standard parametric statistics can be used or not, the normality of
 192 our time series must be assessed first. While non-Gaussian parametric statistics exist, Gaussian
 193 assumptions are common with geophysical time series analysis and are used by the previous
 194 studies on the NA-NP inter-basin relationships (d'Orgeville and Peltier, 2007, Zhang and
 195 Delworth 2007, Wu et al. 2011, Marini and Frankignoul 2014, and Nigam et al. 2020).

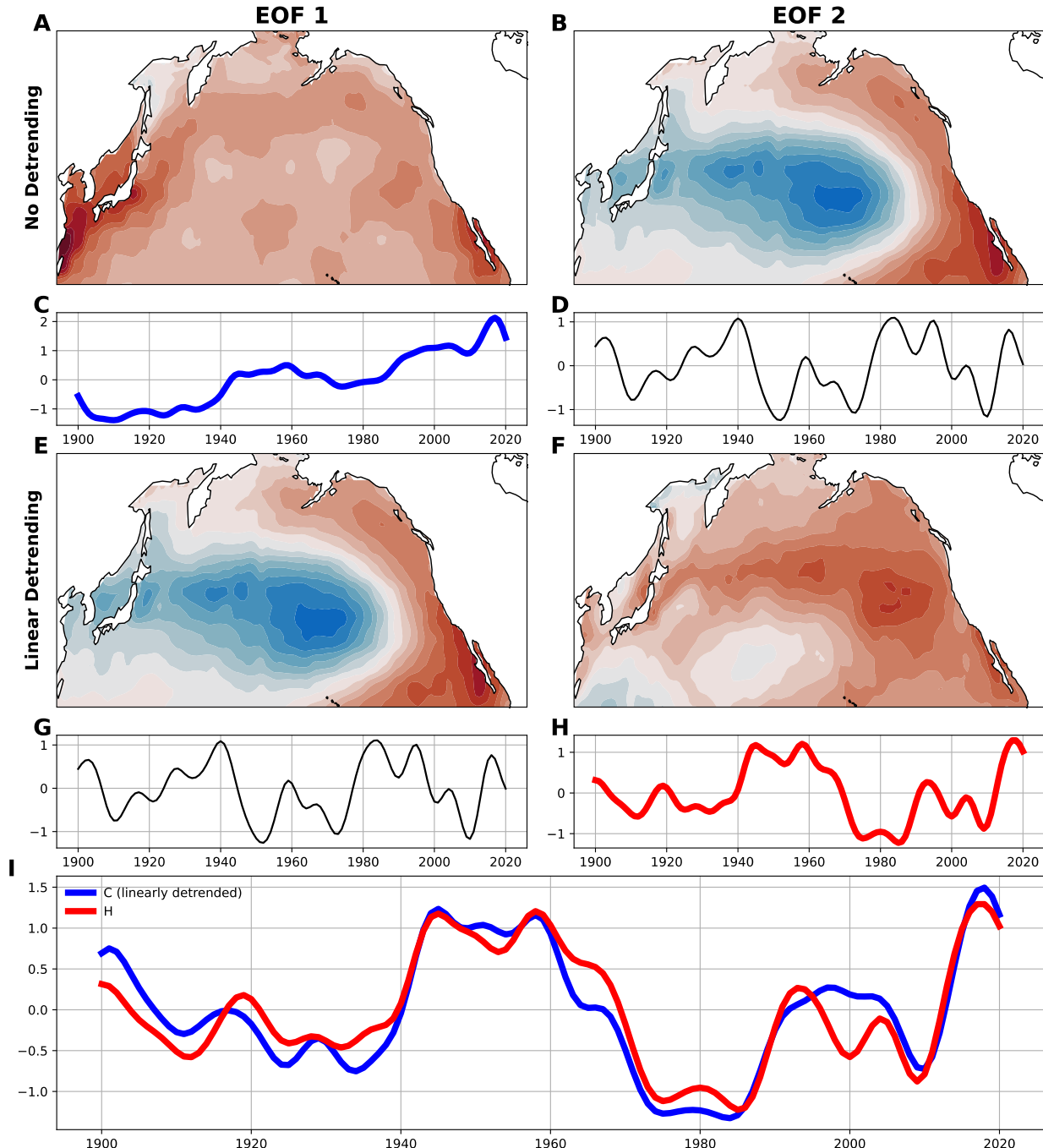
We test the four modes' filtered time series with five normality tests as recommended by Yap and Sim (2011) and Ghasemi and Zahediasl (2012). Two are qualitative assessments: a histogram with a standard normal curve fitted to the data (Figures 1I-L), and a quantile-quantile plot (Figures 1M-P). Three are quantitative: the Shapiro-Wilk test (SW), the D'Agostino skewness test (K^2), and the Anderson-Darling test (AD) (shown as text in Figures 1M-P). Only NP-EOF3 passes more than a single quantitative test. The combination of all tests generally suggests that only NP-EOF3 of the filtered time series can be described as normal, so Gaussian assumptions cannot be made for analysis of mode relationships. Therefore, non-parametric statistics are required for significance testing.

Significance Testing

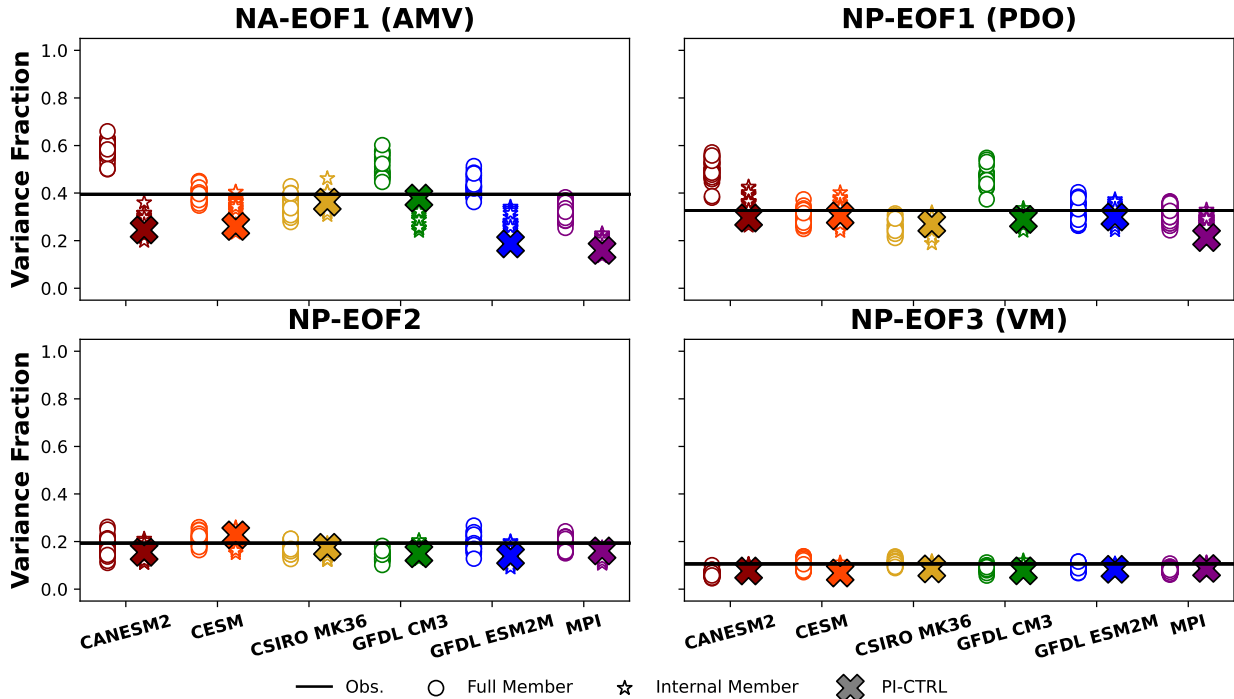
We use a non-parametric bootstrapping method for significance testing. Our primary statistical tool is cross-correlation, so we build this method to evaluate the significance of a given "real" cross-correlation. We create sets of random white-noise time series by shuffling each observed unfiltered time series 1000 times. We also used sets of AR1 red noise (Katz 1982) and quantile-mapped sets (Maraun 2013) and found no qualitative differences in our results. Each random time series is filtered, and each possible pair of modes between each basin is cross-correlated for the entire random set. These 1000 cross-correlations are then used to compute 95% significance thresholds for the corresponding observed cross-correlation. This method is similar to the bootstrap used by Wu et al. (2011), although our method differs slightly. Wu et al. (2011) calculate the 95th percentile at each specific lag in their cross correlation (hereafter the "point test").

Their interest, however, is not on a particular lag, but instead of the peaks of the cross-correlation that are above the significance threshold. The specific lag at which these peaks occurred was unimportant - whether it occurred with 0 year lag or 30 years lag, their conclusions would remain the same. By definition, their statistical test requires that a particular lag be of interest, meaning that the lag at which the peaks occur *is* important, contrary to their conclusions. This can be viewed as an *a priori* test with an *a posteriori* conclusion, which suggests their significance thresholds may not be appropriate.

Alternatively, a "peak test" can be used. Instead of calculating the significance thresholds at each lag, we choose the maximum value of each random cross-correlation to compute the thresholds from. The result is that at 95% confidence, 5% of random cross-correlations have any points that are significant when using the peak test, while ~50% have significant points when using the point test. This shows that using an improper significance test can result in many spurious significant points on any given cross-correlation. All significance thresholds shown here are computed using the peak test.



237
 238 *Figure 2.* The effect linear detrending has on observed EOFs in the NP. For observations where no detrending occurs, A) and C)
 239 show the first EOF spatial pattern and time series respectively. B) and D) show the same but for the second EOF.
 240 For linearly detrended observations, E) and G) show the first EOF spatial pattern and time series respectively, while F) and H)
 241 show the same for the second EOF. I) shows the time series from C) (linearly detrended) and H) together to show their similarity (93%
 242 correlation, significant at the 99% threshold). The red curves are the same time series, while the blue curve in I) is equivalent to
 243 the time series in C) but with the linear slope removed.



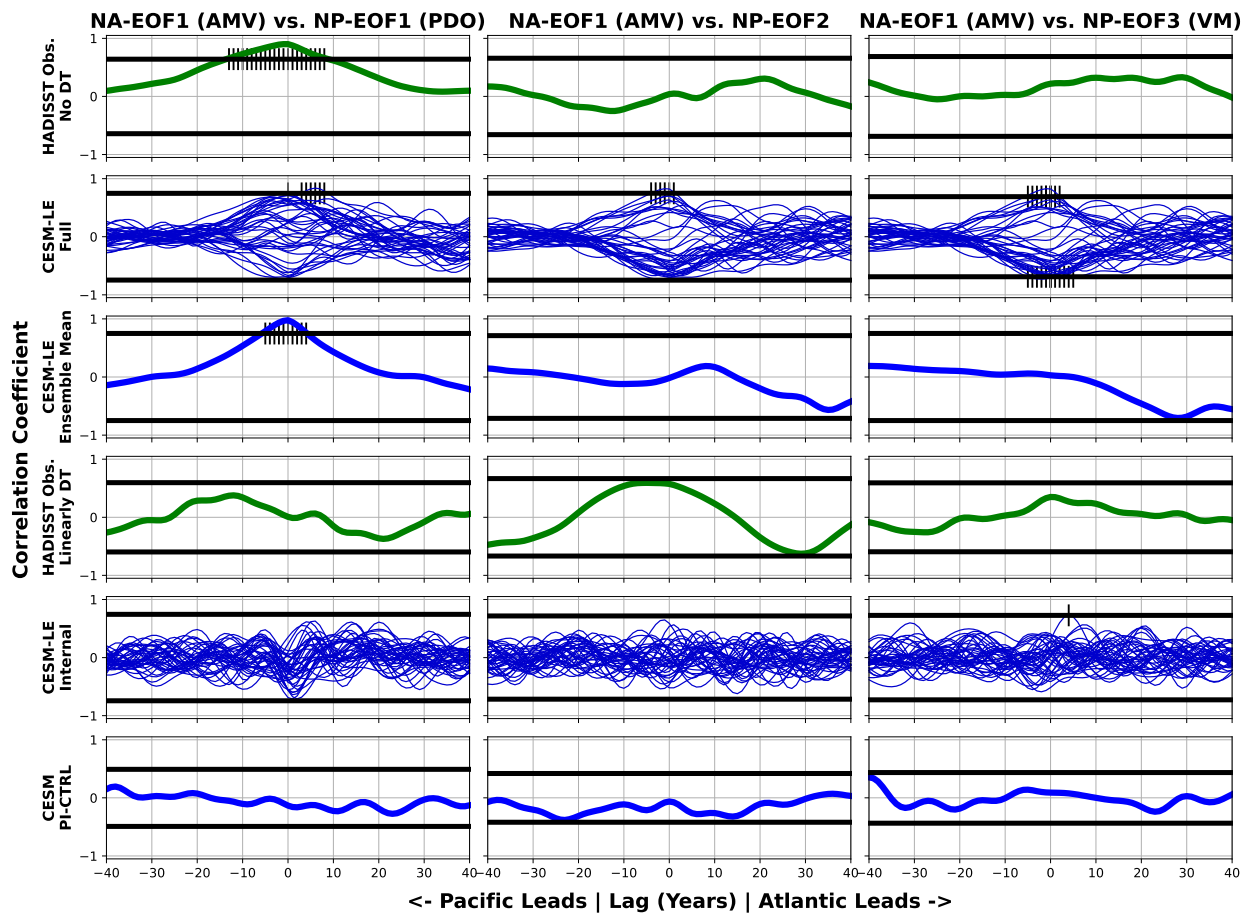
245
 246
 247 Figure 3. EOF variance explained of MMLEA ensemble members. Top row form left to right: NA-EOF1 and NP-EOF1. Bottom
 248 row form left to right: NP-EOF2 and NP-EOF3. Black lines represent observed values. Colors correspond to models as follows:
 249 dark red (CANESM2), orange (CESM), gold (CSIRO MK36), green (GFDL CM3), blue (GFDL ESM2M), and purple (MPI).
 250 For each model, two sub-columns are shown: the full, or total, variability on the left and the internal variability on the right. Each
 251 circle/star represents a single member. Xs represent pre-industrial control values.

252 Results: Model Assessment

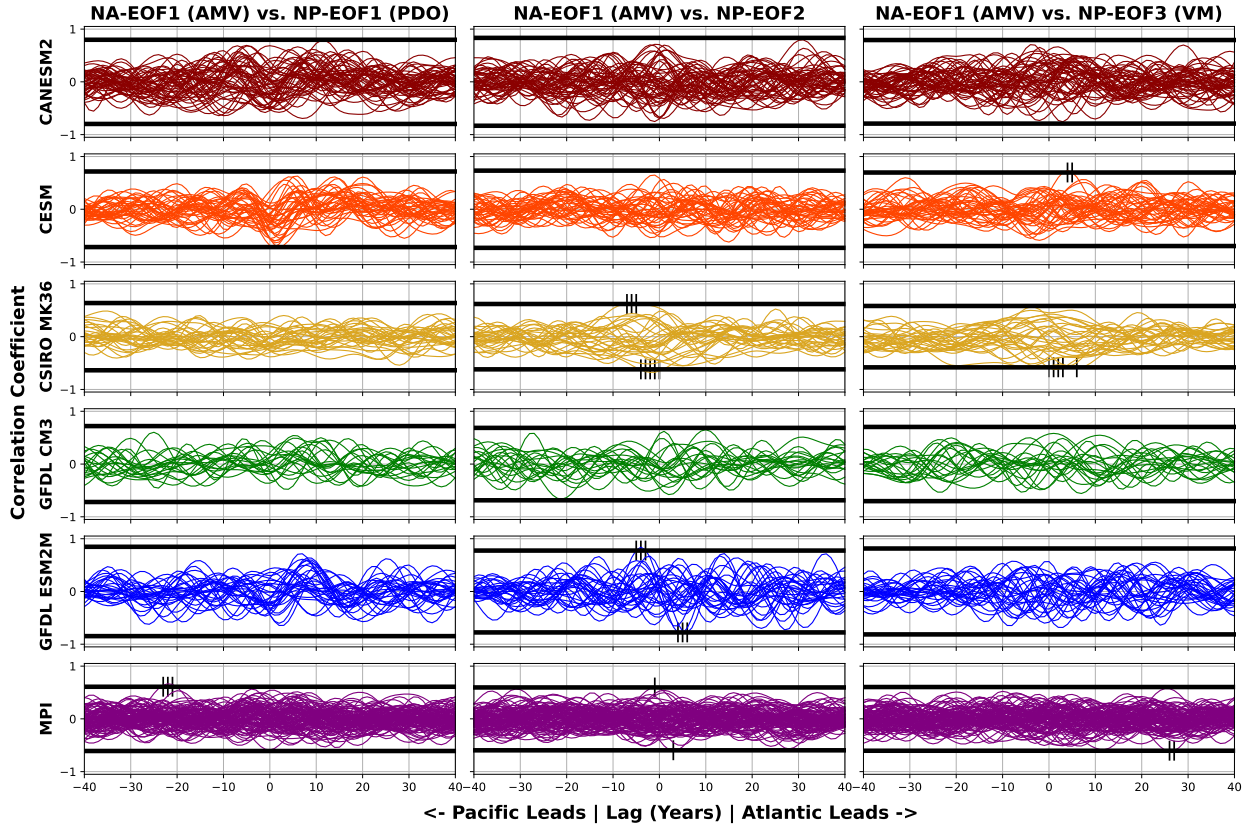
253 Here, we want to assess how realistic the simulated modes are relative to the observed,
 254 including how much of the observed variability can be explained by forcing and internal
 255 variability. One way we can analyze this is to compare the fraction of explained variance for
 256 each EOF to the corresponding value for observations, as shown in Figure . EOF 1 in each basin
 257 shows some inter-model spread, but the observed value falls within the internal range for each
 258 model. For both basins, EOF 1 generally explains between 30-40% variance, while EOF 2
 259 explains 15-20%, and EOF 3 around 10-15%. In some cases for each member, the full variability
 260 explains more variance than its corresponding internal variability. This can be attributed to the
 261 external forcing that is present in the full but not the internal. Generally, the internal variability
 262 should agree with the observations better than the full variability, although both appear relatively
 263 similar to the observed values. The MMLEA looks qualitatively similar enough to observations
 264 for this metric to proceed.

265
 266 We also assess the realism of the MMLE subjectively by looking at the EOF spatial
 267 patterns. Supplemental Figure 2 shows the observed EOFs and the composite mean EOFs for
 268 each model. The MMLEA NA EOFs all roughly share a similar tripole spatial pattern to the
 269 observed first NA-EOF. The magnitude of the gradients across all ensembles differs from the
 270 observations, however. Extending from the Gulf Stream region, the MMLEA models generally
 271 show an opposite trend to the rest of the basin (cooling in the Gulf Stream region when the rest
 272 of the basin is warming), whereas the observations show uniform warming or cooling. In the NP,
 273 NP-EOF1 shows good agreement, all showing the classic PDO pattern. The second observed

274 EOF differs significantly from those in the MMLEA. The observed pattern shows uniform
 275 warming or cooling across the entire basin, while the third observed EOF shows a typical VM
 276 pattern. The MMLEA appears to skip over the uniform warming/cooling spatial pattern, showing
 277 only the PDO as EOF1 and the VM as EOF2 in most members. One possible explanation for this
 278 is that the observed EOF2 represents non-linear features of external forcing, which would
 279 successfully be removed in an MMLEA model by subtracting the ensemble mean, but not in
 280 observations through the linear detrending method. It is interesting that this is different in the
 281 Atlantic and Pacific, suggesting that method for removal of the forced signal is basin dependent.
 282 Generally, the MMLEA members do show internal modes similar to the observed modes (when
 283 comparing observed NP-EOF3 to MMLEA NP-EOF2), suggesting that the models simulate
 284 variability realistically enough to analyze potential mode interactions.



287
 288 Figure 4. Cross-correlations of NA-NP mode relationships. From left to right: AMV (NA-EOF1) vs. PDO (NP-EOF1)
 289 relationship, AMV vs. NP-EOF2 relationship, and AMV vs. VM (NP-EOF3) relationship. From top to bottom: Observations
 290 with no detrending, CESM-LE (from MMLEA) full variability, CESM-LE ensemble mean, Observations with linear detrending,
 291 CESM-LE internal variability, and CESM pre-industrial control variability. Black horizontal lines are 95% statistical significance
 292 thresholds as calculated by the “peak” test. Vertical ticks show where cross-correlations are significant. For positive (negative)
 293 lags, the NA (NP) mode leads. All other MMLEA large ensembles show qualitatively similar results.



294
295 Figure 5. Cross-correlations of MMLEA internal only NA-NP mode relationships. From left to right: AMV (NA-EOF1) vs. PDO
296 (NP-EOF1) relationship, AMV vs. NP-EOF 2, and AMV vs. VM. Black horizontal lines are 95% statistical significance
297 thresholds as calculated by the “peak” test. Vertical ticks show where cross-correlations are significant. For positive (negative)
298 lags, the NA (NP) mode leads. 269 MMLEA members are utilized for a total of 807 relationships. Only 11 (<2%) have
299 statistically significant points.

300 Results: Relationship Analysis

301 Figure 4 shows a series of NA-NP relationships from observations and the CESM Large
302 Ensemble (CESM-LE), one of the MMLEA ensembles. The top row shows the non-detrended
303 (or full) observed EOF cross-correlations. Without detrending, the first EOF of each basin
304 captures the global warming or externally forced signal. The signal in each basin is clearly
305 connected, with significant points along a peak at 0 lag. This can be interpreted as global
306 warming affecting each basin in a very similar way. The other relationships, which capture the
307 internal modes in the NP, show no statistically significant connection.
308

309 The next row shows the relationships for full members of the CESM-LE. Again, most of
310 these relationships show a peak near 0 lag for all three relationships. This suggests that external
311 forcing affects all of the first three NP EOFs, such that a nearly significant peak appears near 0
312 lag for most members. When this global warming signal is shown by itself as the ensemble mean
313 in the third row, the same connection as in the observed forced signals appears, with the forced
314 signal in each basin being significantly correlated. Note that the ensemble mean EOFs 2 and 3 do
315 not have a physical meaning and can be neglected. Also, averaging across all ensemble members
316 may mutually cancel out polarized clusters of members, so caution must be used when
317 computing ensemble means (Bellucci et al. 2017).
318

319 So far, we have shown that the combined internal and forced relationships are statistically
 320 significant, particularly only the forced relationships. Rows four through six analyze only the
 321 internal relationships to determine whether connections between the internal modes exist or not.
 322 Row four shows the linearly detrended observed relationships. The AMV-PDO relationship
 323 (hereafter all relationships referred to as AMV-PDO, AMV-VM, etc.) shows similar results as
 324 Wu et al. (2011), Marini and Frankignoul (2014), and Nigam et al. (2020), and both the AMV-
 325 PDO and AMV-NP-EOF2 show similar results as d'Orgeville and Peltier (2007) and Zhang and
 326 Delworth (2007). However, we show different significance thresholds as per the peak test. The
 327 sign of the correlation and the precise lag at which the maximum correlation occurs may slightly
 328 vary from study to study due to differing methods, particularly the sign of the EOF output and
 329 filter used. Linear detrending is also not ideal for removing the observed forced signal
 330 (Frankignoul et al. 2017), which may allow the forced signal to remain and cause a spurious
 331 higher correlation as seen in AMV-NP-EOF2.

332
 333 To account for the inadequacy of linear detrending, the MMLEA internal relationships and the
 334 CESM PI are shown in rows five and six respectively. Only one of these 120 members show a
 335 significant relationship, suggesting that any internal connection between the NA and NP basins is
 336 indistinguishable from random noise. All other MMLEA ensembles show qualitatively similar
 337 results. Figure 5 shows the internal relationships for all six MMLEA ensembles analyzed, with
 338 only 11 out of 807 (<2%) relationships having any statistically significant points. The same
 339 concept of external forcing driving significant relationships appears in all of the ensembles,
 340 despite their various differences.

342 Discussion

343 Our results suggest that, for the NA and NP basins, an internal connection between the
 344 two does not need consideration as a potential source of variability. These findings may also
 345 have broader implications regarding the roles of external forcing and internal variability as
 346 drivers of climate modes. Present theories on climate mode drivers focus on varying roles for the
 347 ocean, atmosphere, internal variability, and external forcing (e.g. Clement et al. 2015, Newman
 348 et al. 2016, Wills et al. 2018, Zhang et al. 2018, O'Reilly et al. 2019, Zhang et al. 2019, etc.).
 349 External forcing is particularly challenging, due to the direct/linear and indirect/non-linear
 350 effects on climate variability (Frankignoul et al. 2017, Li et al. 2020). Additionally, there is
 351 debate about the role and importance of these internal modes in an increasingly forced global
 352 climate (Ting et al. 2009, DelSole et al. 2011, Haustein et al. 2019, Mann et al. 2020, etc.).

353 Additionally, our results suggest that traditional observed AMV and PDO definitions
 354 contain at least some external forcing. Care must be taken when using these mode definitions to
 355 properly remove the forced signal so as to isolate the internal variability. However, this is a
 356 challenging task outside of the realm of large ensembles. Tools such as the MMLEA will be vital
 357 in making progress toward isolating the forced response in observations, as they can possibly
 358 average out various model differences and provide a closer analog to the observed forced signal.
 359 These modeling tools are especially useful due to the relatively short observed period, which
 360 may not be sufficient to adequately observe variability on multi-decadal timescales, such as those
 361 studied here.

362
 363 Finally, our findings do not rule out other regions or modes driving variability in the NA
 364 and NP. Other mode relationships have been shown to exist, such as how ENSO helps drive the

366 PDO (Newman et al. 2003). Further work can include a complex matrix of potential relationships
 367 between global modes as in Shin et al. (2010) or using global EOFs such as Nigam et al. (2020).
 368 Methods presented here can assist in a thorough decomposition of sources of variability in a
 369 particular region. This can lead to better understanding of variability drivers, which can
 370 ultimately result in improved climate models and more accurate climate forecasts.
 371

372 Acknowledgments, Samples, and Data

373 The authors gratefully acknowledge funding from the NSF Climate and Large Scale Dynamics
 374 program and NOAA Climate Program Office that supported this work. We also acknowledge all
 375 modelling groups and the US CLIVAR Working Group on Large Ensembles for making their
 376 data available in the Multi-Model Large Ensemble data repository. We thank Brian Mapes and
 377 his Applied Data Analysis class for inspiration and discussions on proper statistical analysis.
 378

379 Data Access: <https://www.cesm.ucar.edu/projects/community-projects/MMLEA/> (MMLEA);
 380 <https://www.metoffice.gov.uk/hadobs/hadisst/> (HADISST).

381

382 References

- 383 Alexander, M. A. (2002). The Atmospheric Bridge: The Influence of ENSO Teleconnections on Air–Sea Interaction
 384 over the Global Oceans. *JOURNAL OF CLIMATE*, 15, 27.
- 385 An, X., Wu, B., Zhou, T., & Liu, B. (2021). Atlantic Multidecadal Oscillation Drives Interdecadal Pacific
 386 Variability via Tropical Atmospheric Bridge. *Journal of Climate*, 34(13), 5543–5553.
 387 <https://doi.org/10.1175/JCLI-D-20-0983.1>
- 388 Bellucci, A., Mariotti, A., & Gualdi, S. (2017). The Role of Forcings in the Twentieth-Century North Atlantic
 389 Multidecadal Variability: The 1940–75 North Atlantic Cooling Case Study. *Journal of Climate*, 30(18),
 390 7317–7337. <https://doi.org/10.1175/JCLI-D-16-0301.1>
- 391 Bond, N. A., Overland, J. E., Spillane, M., & Stabeno, P. (2003). Recent shifts in the state of the North Pacific.
 392 *Geophysical Research Letters*, 30(23). <https://doi.org/10.1029/2003GL018597>
- 393 Cane, M. A., Clement, A. C., Murphy, L. N., & Bellomo, K. (2017). Low-Pass Filtering, Heat Flux, and Atlantic
 394 Multidecadal Variability. *Journal of Climate*, 30(18), 7529–7553. <https://doi.org/10.1175/JCLI-D-16-0810.1>
- 395 Clement, A., Bellomo, K., Murphy, L. N., Cane, M. A., Mauritsen, T., Radel, G., & Stevens, B. (2015). The Atlantic
 396 Multidecadal Oscillation without a role for ocean circulation. *Science*, 350(6258), 320–324.
 397 <https://doi.org/10.1126/science.aab3980>
- 398 DelSole, T., Tippett, M. K., & Shukla, J. (2011). A Significant Component of Unforced Multidecadal Variability in
 399 the Recent Acceleration of Global Warming. *Journal of Climate*, 24(3), 909–926.
 400 <https://doi.org/10.1175/2010JCLI3659.1>
- 401 Deser, C., Lehner, F., Rodgers, K. B., Ault, T., Delworth, T. L., DiNezio, P. N., et al. (2020). Insights from Earth
 402 system model initial-condition large ensembles and future prospects. *Nature Climate Change*.
 403 <https://doi.org/10.1038/s41558-020-0731-2>
- 404 Dommeneget, D., & Latif, M. (2008). Generation of hyper climate modes. *Geophysical Research Letters*, 35(2),
 405 L02706. <https://doi.org/10.1029/2007GL031087>
- 406 Eden, C., & Jung, T. (2001). North Atlantic Interdecadal Variability: Oceanic Response to the North Atlantic
 407 Oscillation (1865–1997). *JOURNAL OF CLIMATE*, 14, 16.
- 408 Enfield, D. B., Mestas-Nuñez, A. M., & Trimble, P. J. (2001). The Atlantic Multidecadal Oscillation and its relation
 409 to rainfall and river flows in the continental U.S. *Geophysical Research Letters*, 28(10), 2077–2080.
 410 <https://doi.org/10.1029/2000GL012745>

- 412 Frankignoul, C., Gastineau, G., & Kwon, Y.-O. (2017). Estimation of the SST Response to Anthropogenic and
 413 External Forcing and Its Impact on the Atlantic Multidecadal Oscillation and the Pacific Decadal
 414 Oscillation. *Journal of Climate*, 30(24), 9871–9895. <https://doi.org/10.1175/JCLI-D-17-0009.1>
- 415 Ghasemi, A., & Zahediasl, S. (2012). Normality Tests for Statistical Analysis: A Guide for Non-Statisticians.
 416 *International Journal of Endocrinology and Metabolism*, 10(2), 486–489.
 417 <https://doi.org/10.5812/ijem.3505>
- 418 Haustein, K., Otto, F. E. L., Venema, V., Jacobs, P., Cowtan, K., Hausfather, Z., et al. (2019). A Limited Role for
 419 Unforced Internal Variability in Twentieth-Century Warming. *Journal of Climate*, 32(16), 4893–4917.
 420 <https://doi.org/10.1175/JCLI-D-18-0555.1>
- 421 Katz, R. W. (1982). Statistical Evaluation of Climate Experiments with General Circulation Models: A Parametric
 422 Time Series Modeling Approach. *Journal of Atmospheric Sciences*, 39(7), 1446–1455.
 423 [https://ddoi.org/10.1175/1520-0469\(1982\)039<1446:SEOCEW>2.0.CO;2](https://ddoi.org/10.1175/1520-0469(1982)039<1446:SEOCEW>2.0.CO;2)
- 424 Kay, J. E., Deser, C., Phillips, A., Mai, A., Hannay, C., Strand, G., et al. (2015). The Community Earth System
 425 Model (CESM) Large Ensemble Project: A Community Resource for Studying Climate Change in the
 426 Presence of Internal Climate Variability. *Bulletin of the American Meteorological Society*, 96(8), 1333–
 427 1349. <https://doi.org/10.1175/BAMS-D-13-00255.1>
- 428 Liu, Z., & Alexander, M. (2007). Atmospheric bridge, oceanic tunnel, and global climatic teleconnections. *Reviews
 429 of Geophysics*, 45(2), RG2005. <https://doi.org/10.1029/2005RG000172>
- 430 Lorenzo, E. D., Schneider, N., Cobb, K. M., Franks, P. J. S., Chhak, K., Miller, A. J., et al. (2008). North Pacific
 431 Gyre Oscillation links ocean climate and ecosystem change. *Geophysical Research Letters*, 35(8).
 432 <https://doi.org/10.1029/2007GL032838>
- 433 Mann, M. E., Steinman, B. A., & Miller, S. K. (2020). Absence of internal multidecadal and interdecadal
 434 oscillations in climate model simulations. *Nature Communications*, 11(1), 49.
 435 <https://doi.org/10.1038/s41467-019-13823-w>
- 436 Mann, M. E., Steinman, B. A., Brouillette, D. J., & Miller, S. K. (2021). Multidecadal climate oscillations during the
 437 past millennium driven by volcanic forcing. *Science*, 371(6533), 1014–1019.
 438 <https://doi.org/10.1126/science.abc5810>
- 439 Mantua, N. J., Hare, S. R., Zhang, Y., Wallace, J. M., & Francis, R. C. (1997). A Pacific Interdecadal Climate
 440 Oscillation with Impacts on Salmon Production*. *Bulletin of the American Meteorological Society*, 78(6),
 441 1069–1080. [https://doi.org/10.1175/1520-0477\(1997\)078<1069:APICOW>2.0.CO;2](https://doi.org/10.1175/1520-0477(1997)078<1069:APICOW>2.0.CO;2)
- 442 Maraun, D. (2013). Bias Correction, Quantile Mapping, and Downscaling: Revisiting the Inflation Issue. *Journal of
 443 Climate*, 26(6), 2137–2143. <https://doi.org/10.1175/JCLI-D-12-00821.1>
- 444 Marini, C., & Frankignoul, C. (2014). An attempt to deconstruct the Atlantic Multidecadal Oscillation. *Climate
 445 Dynamics*, 43(3), 607–625. <https://doi.org/10.1007/s00382-013-1852-3>
- 446 Martin, T., Reintges, A., & Latif, M. (2019). Coupled North Atlantic Subdecadal Variability in CMIP5 Models.
 447 *Journal of Geophysical Research: Oceans*, 124(4), 2404–2417. <https://doi.org/10.1029/2018JC014539>
- 448 Newman, M., Compo, G. P., & Alexander, M. A. (2003). ENSO-Forced Variability of the Pacific Decadal
 449 Oscillation. *JOURNAL OF CLIMATE*, 16, 5.
- 450 Newman, M., Alexander, M. A., Ault, T. R., Cobb, K. M., Deser, C., Di Lorenzo, E., et al. (2016). The Pacific
 451 Decadal Oscillation, Revisited. *Journal of Climate*, 29(12), 4399–4427. [https://doi.org/10.1175/JCLI-D-15-0508.1](https://doi.org/10.1175/JCLI-D-15-

 452 0508.1)
- 453 Nigam, S., Sengupta, A., & Ruiz-Barradas, A. (2020). Atlantic–Pacific Links in Observed Multidecadal SST
 454 Variability: Is the Atlantic Multidecadal Oscillation’s Phase Reversal Orchestrated by the Pacific Decadal
 455 Oscillation? *Journal of Climate*, 33(13), 5479–5505. <https://doi.org/10.1175/JCLI-D-19-0880.1>
- 456 O'Reilly, C. H., Zanna, L., & Woollings, T. (2019). Assessing External and Internal Sources of Atlantic
 457 Multidecadal Variability Using Models, Proxy Data, and Early Instrumental Indices. *Journal of Climate*,
 458 32(22), 7727–7745. <https://doi.org/10.1175/JCLI-D-19-0177.1>
- 459 d'Orgeville, M., & Peltier, W. R. (2007). On the Pacific Decadal Oscillation and the Atlantic Multidecadal
 460 Oscillation: Might they be related?: PDO AND AMO RELATED? *Geophysical Research Letters*, 34(23),
 461 n/a-n/a. <https://doi.org/10.1029/2007GL031584>
- 462 Qin, M., Dai, A., & Hua, W. (2020). Quantifying contributions of internal variability and external forcing to Atlantic
 463 multidecadal variability since 1870. *Geophysical Research Letters*. <https://doi.org/10.1029/2020GL089504>
- 464 Raible, C. C., Lehner, F., González-Rouco, J. F., & Fernández-Donado, L. (2014). Changing correlation structures
 465 of the Northern Hemisphere atmospheric circulation from 1000 to 2100 AD. *Climate of the Past*, 10(2),
 466 537–550. <https://doi.org/10.5194/cp-10-537-2014>

- 467 Rayner, N. A. (2003). Global analyses of sea surface temperature, sea ice, and night marine air temperature since the
468 late nineteenth century. *Journal of Geophysical Research*, 108(D14), 4407.
469 <https://doi.org/10.1029/2002JD002670>
- 470 Salinger, M. J., Renwick, J. A., & Mullan, A. B. (2001). Interdecadal Pacific Oscillation and South Pacific climate.
471 *International Journal of Climatology*, 21(14), 1705–1721. <https://doi.org/10.1002/joc.691>
- 472 Shin, S.-I., Sardeshmukh, P. D., & Pegion, K. (2010). Realism of local and remote feedbacks on tropical sea surface
473 temperatures in climate models. *Journal of Geophysical Research*, 115(D21), D21110.
474 <https://doi.org/10.1029/2010JD013927>
- 475 Ting, M., Kushnir, Y., Seager, R., & Li, C. (2009). Forced and Internal Twentieth-Century SST Trends in the North
476 Atlantic. *Journal of Climate*, 22(6), 1469–1481. <https://doi.org/10.1175/2008JCLI2561.1>
- 477 Wills, R. C., Schneider, T., Wallace, J. M., Battisti, D. S., & Hartmann, D. L. (2018). Disentangling Global
478 Warming, Multidecadal Variability, and El Niño in Pacific Temperatures. *Geophysical Research Letters*,
479 45(5), 2487–2496. <https://doi.org/10.1002/2017GL076327>
- 480 Wills, R. C. J., Armour, K. C., Battisti, D. S., & Hartmann, D. L. (2019). Ocean–Atmosphere Dynamical Coupling
481 Fundamental to the Atlantic Multidecadal Oscillation. *Journal of Climate*, 32(1), 251–272.
482 <https://doi.org/10.1175/JCLI-D-18-0269.1>
- 483 Wu, S., Liu, Z., Zhang, R., & Delworth, T. L. (2011). On the observed relationship between the Pacific Decadal
484 Oscillation and the Atlantic Multi-decadal Oscillation. *Journal of Oceanography*, 67(1), 27–35.
485 <https://doi.org/10.1007/s10872-011-0003-x>
- 486 Yap, B. W., & Sim, C. H. (2011). Comparisons of various types of normality tests. *Journal of Statistical
487 Computation and Simulation*, 81(12), 2141–2155. <https://doi.org/10.1080/00949655.2010.520163>
- 488 Zhang, R., & Delworth, T. L. (2007). Impact of the Atlantic Multidecadal Oscillation on North Pacific climate
489 variability: IMPACT ON NORTH PACIFIC VARIABILITY. *Geophysical Research Letters*, 34(23), n/a-
490 n/a. <https://doi.org/10.1029/2007GL031601>
- 491 Zhang, R., Sutton, R., Danabasoglu, G., Kwon, Y., Marsh, R., Yeager, S. G., et al. (2019). A Review of the Role of
492 the Atlantic Meridional Overturning Circulation in Atlantic Multidecadal Variability and Associated
493 Climate Impacts. *Reviews of Geophysics*, 2019RG000644. <https://doi.org/10.1029/2019RG000644>
- 494 Zhang, Y., Xie, S.-P., Kosaka, Y., & Yang, J.-C. (2018). Pacific Decadal Oscillation: Tropical Pacific Forcing
495 versus Internal Variability. *Journal of Climate*, 31(20), 8265–8279. [https://doi.org/10.1175/JCLI-D-18-0164.1](https://doi.org/10.1175/JCLI-D-18-
496 0164.1)
- 497